PROCEEDINGS OF SCIENCE

A multi-detector EAS reconstruction framework for IceCube

The IceCube Collaboration

(a complete list of authors can be found at the end of the proceedings)

E-mail: agnlesz@udel.edu, alan.coleman@physics.uu.se, matthias.plum@sdsmt.edu

The IceCube Neutrino Observatory is also a very unique extensive air shower (EAS) detector, that simultaneously measures the EAS footprint on the surface and the high-energy muons in deep ice. The surface array - IceTop, comprising of ice-Cherenkov tanks, will be enhanced in the coming years with scintillation detectors and radio antennas. The hybrid detection enables the reconstruction of EAS parameters based on different underlying signal distributions. A new framework within the IceCube software allows for a flexible implementation of signal and time models for different detector components and a combination of resulting likelihood functions. The in-ice muon signal can serve as an anchor for the reconstruction of the EAS axis, resulting in an improved reconstruction resolution. Moreover, it makes it possible to reconstruct EASs with an impact point outside the IceTop array, opening a larger zenith-angle range for analyses of IceTop and in-ice coincident events. In this contribution, we present the capabilities of the combined reconstruction for different classes of EAS events with various detector configurations.

Corresponding authors: Agnieszka Leszczynska[1*], Alan Coleman[1,2], Matthias Plum[3], Dennis Soldin[4,5]

[1] *Bartol Research Institute and Dept. of Physics and Astronomy, University of Delaware, Newark, DE 19716, USA*

[2] *Dept. of Physics and Astronomy, Uppsala University, Box 516, S-75120 Uppsala, Sweden*

[3] *South Dakota School of Mines & Technology, Rapid City, SD, USA*

[4] *Karlsruhe Institute of Technology, Institute of Experimental Particle Physics, Karlsruhe, Germany*

[5] *Department of Physics and Astronomy, University of Utah, Salt Lake City, UT 84112, USA*

[*] Presenter

The 38th International Cosmic Ray Conference (ICRC2023)
26 July – 3 August, 2023
Nagoya, Japan

© Copyright owned by the author(s) under the terms of the Creative Commons Attribution-NonCommercial-NoDerivatives 4.0 International License (CC BY-NC-ND 4.0).

PoS(ICRC2023)366

1. Introduction

Over the last decades, EAS experiments have been continuously improving their detection and calibration techniques, as well as the accuracy of the measurements. The results of EAS arrays and particle accelerators have deepened our understanding of the air-shower development, allowing for better modeling of the particle distributions, and in turn more precise estimations of the primary cosmic-ray (CR) properties [1]. Further improvements can be achieved by probing different EAS components simultaneously with different detector types. The IceCube Neutrino Observatory is already uniquely equipped to detect not only the footprint of abundant particles on the surface, but also the high-energy muons ($\gtrsim 300\,\mathrm{GeV}$) penetrating the in-ice optical array. The surface part of IceCube, IceTop, an array of ice-Cherenkov tanks, detects mainly electromagnetic particles and low-energy muons. It provides a good estimate of the CR energy and EAS geometry for events that are well-contained within the $1\,\mathrm{km}^2$ array [2]. For EAS experiments, the CR mass is typically inferred using measurements of the muon content in the air shower or the atmospheric depth of the maximum number of particles; it also impacts the shape of the particle distributions on the ground. Measurements of the $\sim 1\,\mathrm{GeV}$ muon content are performed using IceTop [3], and the high-energy muons ($\gtrsim 300\,\mathrm{GeV}$) are measured with the in-ice array. The CR composition analysis at IceCube is currently obtained using mainly the in-ice signals [2]. However, to provide information from both IceTop and the in-ice array, only events intersecting both detectors can be analyzed, significantly limiting the accessible solid angle. This could be solved by utilizing, in the EAS reconstruction, the high-energy muons which closely follow the EAS axis, opening the possibility to reconstruct events that are not well contained within the IceTop array [4].

IceTop is planned to be enhanced with additional detector types, scintillation detectors and radio antennas [5]. The response of the scintillator panels and IceTop tanks to the various classes of secondary particles is different, and the overall variations between these detectors result in small differences in the observed lateral distributions. Orthogonally, the radio antennas can detect the radio-frequency emission that is generated by moving charged EAS particles. This technique provides a good estimate of the atmospheric depth of the maximal number of electromagnetic particles (X_{max}) as well as a measurement of the electromagnetic EAS energy. The multi-detector measurements will allow us to study air showers from complementary perspectives. Additional measurement points can improve the current reconstruction accuracy, as well as extend the event sample. This motivated the effort to create a common framework for multi-detector EAS reconstruction at IceCube - a code structure that is flexible enough to accommodate any combination of the detector components depending on the class of events.

In this work, we study two classes of events. The first comprises *contained* events, those that have their EAS axis passing through the surface array. All IceTop analyses exclusively use events that are selected based on this containment criterion. The second class comprises *uncontained* events. This set generally contains the EASs that produce signals in the IceTop tanks and are not limited by the containment criterion. However, in this work, we will adopt the definition that uncontained events have some signals in both, the surface and the in-ice detectors.

PoS(ICRC2023)366

2. Reconstruction framework

The basis of this new framework is a construction of the likelihoods and parameter space for individual detector-arrays and linking them into one global minimization. The expected response of any individual array can be modeled by a distribution of signal strengths and arrival times in the EAS coordinate system (refer to as the *lateral distribution function*, or LDF, and the *EAS front*), as well as their respective probability distributions. These model functions are generic and can be populated with user-defined values. All the likelihood functions and models are derived from the same base class, such that new detectors and reconstructions can be easily added. During the fitting routine, the hypothesis of the geometry of the EAS (orientation and trajectory) is given to each array's likelihood routine, from which the expected signals and timing can be calculated using that array's LDF and EAS front expectation. From this, the likelihoods from all the detector components (involved in a given reconstruction) of the current event hypothesis are combined.

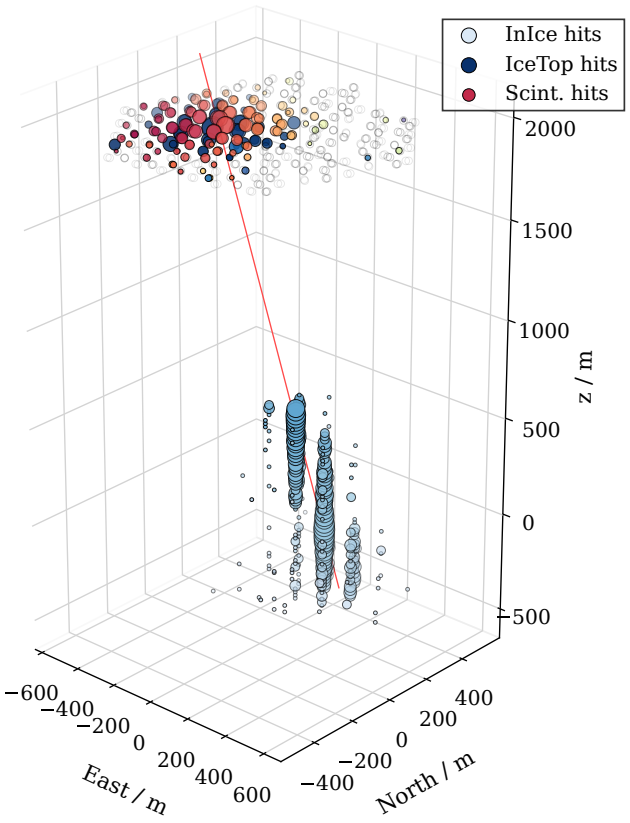

Figure 1: Example of a contained multi-detector EAS-event simulation. Signals at the surface from IceTop tanks and below the surface from the optical array are marked in blue, and from the scintillation detectors in maroon. The shades indicate the arrival times, and the size of the markers scales with signal strength. No background noise is plotted. The red line indicates the EAS axis. The radio signals are not shown.

Two limited sets of simulated EAS events propagated through different detector arrays were prepared to study the capabilities of this multi-detector reconstruction. The IceTop enhancement assumes 32 stations of 8 scintillation detectors and 3 radio antennas [5]. All EASs were generated using CORSIKA [6] with FLUKA [7, 8] and Sibyll 2.3d [9] for low- and high-energy hadronic interactions, respectively. The radio emission generated by the EASs was simulated using CoREAS [10]. The energy depositions from the EAS particles in the IceTop tanks and scintillation detectors were calculated with the Geant4 toolkit [11], for details see [12, 13]. IceTop has a time-dependent nature due to the snow accumulation on top of the tanks [14]. The tanks were thus simulated with snow heights extrapolated for the year 2025 from previous years' measurements at the South Pole, resulting in an overburden of ≈3.3 m of snow on average. High-energy muons were propagated in the ice using PROPOSAL [15], and photon propagation to the optical modules was done with a simulation package based on OpenCL [16] embedded in the IceCube software. The simulation of the antennas generally follows the scheme

PoS(ICRC2023)366

outlined in [17]. The voltage waveforms were generated by folding in the response of the SKALAv2 antennas [18] with the simulated electric fields via an interpolation method. Likewise, the response of the readout electronics (cables, amplifiers, digitizer, etc.) was included to produce realistic waveforms. Noise was added to the waveforms using a combination of Johnson-Nyquist noise and the Cane model of (extra-)galactic emission [19].

An example of a multi-detector simulated event induced by a 10 PeV proton is shown in Figure 1. The colors reflect the arrival times, while the sizes of the markers indicate the signal strength. The EAS axis, marked as a red line, is well anchored by the in-ice array response. The addition of the scintillation detectors increases sampling of the particle footprint close to the impact point and extends it to larger distances.

For simulating contained events, CORSIKA simulations were re-sampled ten times with impact points randomly distributed on a circle with a 400 m radius from the IceTop center. For the uncontained case, the impact points were chosen randomly within 1 km distance from the IceTop border and the EAS axis was chosen to pass through the in-ice volume to maximize the event generation. This volume is defined by a 3D convex hull that encloses all but the outer layer of the in-ice detectors.

3. Reconstruction using multiple detectors

For both the contained and uncontained events, the multi-detector reconstruction method yields improved resolutions on the EAS parameters. It should be noted that with a multi-detector reconstruction, the quantity of the minimization settings (step sizes, boundaries etc.) is essentially a separate optimization problem, and here we report only the currently selected version.

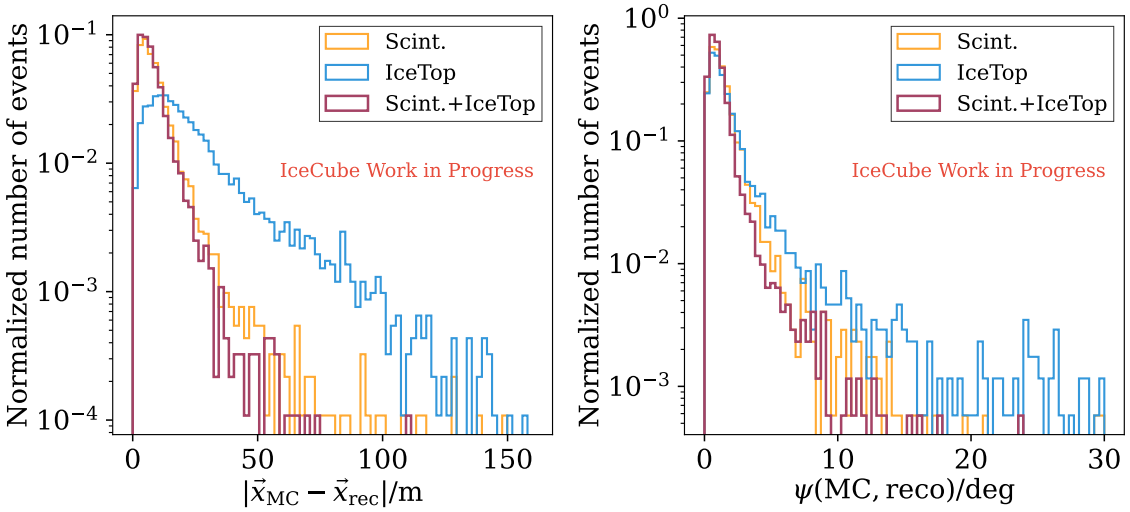

Figure 2: Reconstruction performance for single (IceTop/scintillator array) and combined reconstructions. Left: the displacement of the simulated vs reconstructed impact points. Right: the angle between the simulated and reconstructed arrival directions. The resolution using only the IceTop tanks (blue) and scintillator panels (yellow) is shown, along with the reconstruction using the combined information (maroon).

PoS(ICRC2023)366

3.1 Contained events with IceTop and scintillation detectors

An increased number of sampling points, by including different detectors, can improve the EAS geometry reconstruction, which in turn improves the reconstruction of physics-relevant observables such as CR energy and mass. We first studied the improvement using only surface information, i.e. from IceTop and scintillator array (and their combination) as most air showers, particularly the inclined ones, do not have corresponding in-ice signals. For this study, we use proton-induced EASs with PeV energies and zenith angles ranging from vertical up to 45°. Both arrays' reconstructions use LDF in this form: $S(r) = S_{ref}\,(r/R_{ref})^{-\beta-\kappa\log_{10}(r/R_{ref})}$, where R_{ref} is a reference distance and S_{ref} is expected signal at this distance. The scintillator EAS front is described by a simple parabolic shape, while IceTop one has additional Gaussian structure close to the axis. For more details about the models and the likelihood functions see [20] and [12].

Figure 2 shows the reconstruction performance on the parameters that define the EAS axis. The improvement when combining information from two arrays is clearly visible for both variables, particularly for the tails in the distribution of the impact-point differences. For these ≈1 PeV events, the resolution (defined as the 68th percentile) of the impact point for the combined reconstruction improves by ∼ 1 m with respect to the scintillator-only case, and almost 20 m with respect to the IceTop-only one. The larger improvement for IceTop is expected since 1 PeV is below the full efficiency of the array for the simulated snow heights, and thus individual events include only a few tanks. At higher energies, 10 PeV, the resolutions of the EAS impact point and direction are even better, 4 m and 0.5°, for the combined reconstruction.

When combining different arrays in one minimization routine, one of the difficulties is that the hypothesis of the EAS arrival time is shared. Ideally, the reconstruction of the EAS front would describe when the first particles arrived at/near a given detector. However, due to the timing delays in the detector's response (e.g. from cables, digitization, light collection time, etc.), sharing a common time-base requires detailed knowledge of the detector response and readout hardware. Only some of these time delays have been incorporated for the scintillator simulation, since the operational settings have not been finalized. So for the combined reconstruction with the IceTop tanks, an extra parameter was fit to account for a time offset relative to the EAS arrival time.

3.2 Impact on the resolution of X_{max}

The reconstruction of events using radio antennas requires a good estimate of the position and orientation of the EAS axis. Unlike in the case of the particle detectors, the lateral distribution of the radio emission is non-monotonic. The coherent emission is beamed at the Cherenkov angle and produces a ring of enhanced emission. For the South Pole, these Cherenkov peaks occur at distances of up to hundreds of meters [21].

Events were reconstructed using a model for the reconstructed energy fluence (energy-per-area) that is received by the antenna. This is done by unfolding the antenna response function from the observed voltage waveforms. This procedure, described in [17], produces an estimate of the electric field components at the antenna location. The likelihood is then calculated by transforming into the $\hat{v} \times \hat{B}$ coordinate system, where v is the propagation direction and B is the local magnetic field (see e.g. [22]), and calculating the fluence of the $\hat{v} \times \hat{B}$ and $\hat{v} \times (\hat{v} \times \hat{B})$ components of the electric field.

PoS(ICRC2023)366

These observed energy fluences are compared to the expected one given by an LDF, whose shape depends only on an overall normalization and the slant depth from the observation point to $X_{\max}$ [21]. Using such a formalism, the reconstruction directly produces the two parameters of interest, $X_{\max}$ and the total amount of radiated energy, of which the latter is proportional to the number of electrons and positrons in the air shower.

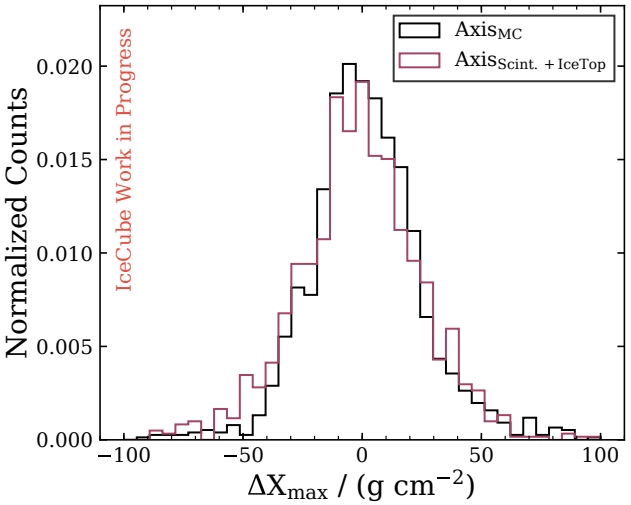

Figure 3: The resolution on $X_{\max}$, as reconstructed using the radio antennas, is shown for 50 PeV air showers. During the reconstruction, the EAS axis was fixed to either the reconstructed or true (MC) one.

Figure 3 shows the resolution on the reconstructed $X_{\max}$ values for 50 PeV EASs with zenith angles of 45°–57° using this likelihood method. The reconstructions have been performed by using the EAS axis identified by either the true one (MC) or the one from the combined surface reconstruction, as detailed in section 3.1. The reconstructions on $X_{\max}$ are 20.3 ± 0.6 g/cm^2 when using the true EAS axis and 24.9 ± 0.8 g/cm^2 when using the axis from the combined reconstruction. That the resolution of the combined reconstruction is almost as good as that of using the true impact point is unsurprising as there are many tens of detectors triggered in both arrays. In these cases, the large amount of data ensures a high-quality reconstruction with a resolution of the EAS impact point and direction of 5 m and 0.5°, respectively.

3.3 Uncontained events with the in-ice array

Uncontained events, in general, refer to air showers that impact the surface outside of the IceTop boundary. They pose a challenge for data analysis because the surface detectors are not capturing sufficient information about the EAS footprint. Hence, relevant observables, such as CR energy, are underestimated or distorted as there is a degeneracy between the reconstructed impact parameter and the EAS size. However, the reconstruction using the combination of surface and in-ice information can break this degeneracy. In this study, we first infer the impact point on the surface from the in-ice reconstructed axis, and then combine surface and in-ice signals in a minimization routine.

Since most of the particles in uncontained events land outside of the surface array, the energy threshold to trigger IceTop increases and depends on the zenith angle, θ. For this study, only EAS simulations with an energy of 10 PeV and a zenith angle up to 40° were considered. The difference between simulated and reconstructed impact points and directions, using IceTop-only as well as IceTop and in-ice combined reconstruction, are shown in figure 4. Only events with an impact point outside of IceTop were selected. However, due to the applied pulse cleaning they span only up to $\simeq 100$ m from the array border. The resolution with a combined reconstruction improves by around 30% for these events. Further work on adjusting the current processing will allow for an extension of the event sample to larger distances.

PoS(ICRC2023)366

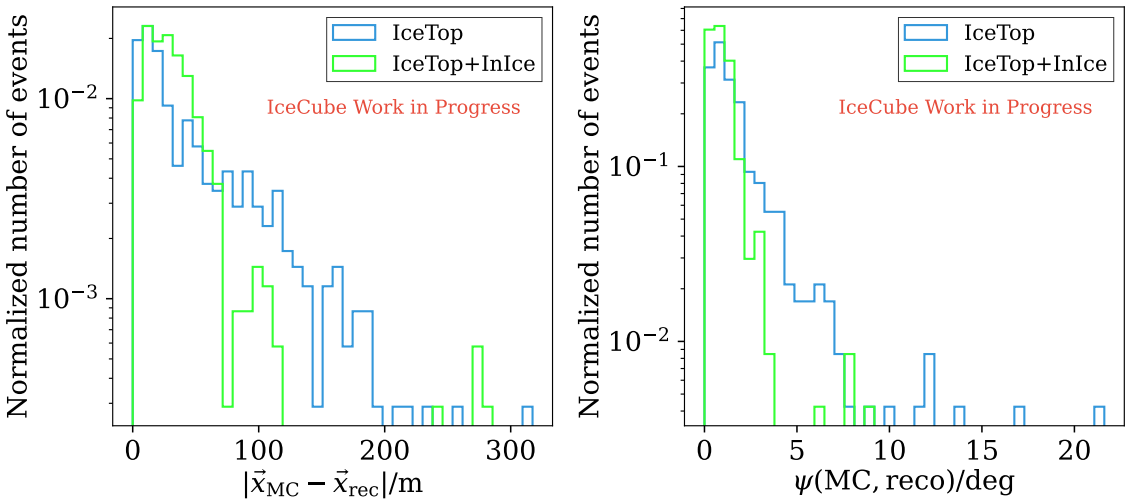

Figure 4: Reconstruction performance for uncontained events that use signals from IceTop-only as well as from the in-ice detectors. Left: the displacement of the simulated vs reconstructed impact points. Right: the angle between the simulated and reconstructed arrival directions.

4. Outlook

The distinctive construction of IceTop, located above the in-ice detector array, enables the analysis of the events that are not contained within the IceTop area by including the in-ice signals from high-energy muons. Moreover, the planned IceTop enhancement foresees the deployment of scintillation panels and radio antennas, which will provide additional information about the EAS footprint. A new reconstruction framework allows us to effectively combine all measured data in a minimization routine of a negative log-likelihood. A preliminary hybrid reconstruction based on IceTop and the planned scintillator array shows an improvement in the estimation of EAS geometric parameters, which translates to the CR observables' resolutions. The EASs which are not contained within the IceTop array typically would not be included for further analysis due to deteriorated reconstruction. Utilizing the in-ice track reconstruction and combining it with the IceTop one, allows for successful reconstruction of these events. While a more systematic investigation is required, this study demonstrates the feasibility to include uncontained events in EAS analyses.

Another reconstruction technique that this framework allows for is the use of multiple LDFs to describe a single array's observations of a given event. Such a technique is currently being explored to describe the total observed signal in the IceTop tanks as the combination of a muon and electromagnetic LDF [23]. Such a technique enables measurements of the muon content in EASs on an event-by-event basis.

Future work will explore the possibility to reconstruct sub-threshold events wherein there are not enough triggered detectors in a single array to fully constrain the EAS axis and the LDF. While the scintillator array requires at least five detectors and IceTop at least five pairs of neighboring tanks, it would be possible with this reconstruction framework to recover these sub-threshold events by the combination of information from both arrays. This would enhance the number of both low-energy and high zenith-angle events where the scintillator array and IceTop have better efficiency, respectively.

PoS(ICRC2023)366

References

[1] A. Coleman *et al.* *Astropart. Phys.* **149** (2023) 102819.

[2] **IceCube** Collaboration, M. G. Aartsen *et al.* *Phys. Rev. D* **100** (Oct, 2019) 082002.

[3] **IceCube** Collaboration, R. Abbasi *et al.* *Phys. Rev. D* **106** (Aug, 2022) 032010.

[4] **IceCube** Collaboration, X. Bai, E. Dvorak, J. Gonzalez, and D. Soldin *PoS* **ICRC2019** (2020) 244.

[5] **IceCube** Collaboration, Shefali and F. G. Schroeder *PoS* **ICRC2023** (these proceedings) 342.

[6] D. Heck *et al.*, "CORSIKA: A monte carlo code to simulate extensive air showers," tech. rep., 1998. 51.02.03; LK 01; Wissenschaftliche Berichte, FZKA-6019 (Februar 98).

[7] A. Ferrari, P. R. Sala, A. Fasso, and J. Ranft. CERN-2005-10, SLAC-R-773 (2005).

[8] T. T. Böhlen *et al.* *Nucl. Data Sheets* **120** (2014) 211–214.

[9] F. Riehn, R. Engel, A. Fedynitch, T. K. Gaisser, and T. Stanev *Phys. Rev. D* **102** (Sep, 2020) 063002.

[10] T. Huege, M. Ludwig, and C. W. James *AIP Conf. Proc.* **1535** no. 1, (2013) 128.

[11] **GEANT4** Collaboration, S. Agostinelli *et al.* *Nucl. Instrum. Meth.* **A506** (2003) 250–303.

[12] **IceCube** Collaboration, R. Abbasi *et al.* *Nucl. Instrum. Meth. A* **700** (2013) 188–220.

[13] **IceCube** Collaboration, A. Leszczyńska and M. Plum *PoS* **ICRC2019** (2020) 332.

[14] **IceCube** Collaboration, K. Rawlins *PoS* **ICRC2015** (2016) 628.

[15] J.-H. Koehne *et al.* *Computer Physics Communications* **184** no. 9, (2013) 2070–2090.

[16] "Github: clsim." `https://github.com/claudiok/clsim`. Accessed: 2023-06-27.

[17] **IceCube** Collaboration, R. Abbasi *et al.* *JINST* **17** no. 06, (2022) P06026.

[18] E. De Lera Acedo *et al.* *Proceedings of ICEAA 2015* (Sep., 2015) 839–843.

[19] H. V. Cane *Mon. Not. R. Astron. Soc.* **189** no. 3, (1979) 465–478.

[20] A. S. Leszczyńska, *Potential of the IceTop Enhancement with a Scintillation Detector Array*. Phd thesis, Karlsruhe Institute of Technology, 2021.

[21] A. Coleman *PoS* **ARENA2022** (2023) 038.

[22] E. N. Paudel, A. Coleman, and F. G. Schroeder *Phys. Rev. D* **105** no. 10, (2022) 103006.

[23] **IceCube** Collaboration, M. Weyrauch and D. Soldin *PoS* **ICRC2023** (these proceedings) 357.

PoS(ICRC2023)366

Full Author List: IceCube Collaboration

R. Abbasi[17], M. Ackermann[63], J. Adams[18], S. K. Agarwalla[40, 64], J. A. Aguilar[12], M. Ahlers[22], J.M. Alameddine[23], N. M. Amin[44], K. Andeen[42], G. Anton[26], C. Argüelles[14], Y. Ashida[53], S. Athanasiadou[63], S. N. Axani[44], X. Bai[50], A. Balagopal V.[40], M. Baricevic[40], S. W. Barwick[30], V. Basu[40], R. Bay[8], J. J. Beatty[20, 21], J. Becker Tjus[11, 65], J. Beise[61], C. Bellenghi[27], C. Benning[1], S. BenZvi[52], D. Berley[19], E. Bernardini[48], D. Z. Besson[36], E. Blaufuss[19], S. Blot[63], F. Bontempo[31], J. Y. Book[14], C. Boscolo Meneguolo[48], S. Böser[41], O. Botner[61], J. Böttcher[1], E. Bourbeau[22], J. Braun[40], B. Brinson[6], J. Brostean-Kaiser[63], R. T. Burley[2], R. S. Busse[43], D. Butterfield[40], M. A. Campana[49], K. Carloni[14], E. G. Carnie-Bronca[2], S. Chattopadhyay[40, 64], N. Chau[12], C. Chen[6], Z. Chen[55], D. Chirkin[40], S. Choi[56], B. A. Clark[19], L. Classen[43], A. Coleman[61], G. H. Collin[15], A. Connolly[20, 21], J. M. Conrad[15], P. Coppin[13], P. Correa[13], D. F. Cowen[59, 60], P. Dave[6], C. De Clercq[13], J. J. DeLaunay[58], D. Delgado[14], S. Deng[1], K. Deoskar[54], A. Desai[40], P. Desiati[40], K. D. de Vries[13], G. de Wasseige[37], T. DeYoung[24], A. Diaz[15], J. C. Díaz-Vélez[40], M. Dittmer[43], A. Domi[26], H. Dujmovic[40], M. A. DuVernois[40], T. Ehrhardt[41], P. Eller[27], E. Ellinger[62], S. El Mentawi[1], D. Elsässer[23], R. Engel[31, 32], H. Erpenbeck[40], J. Evans[19], P. A. Evenson[44], K. L. Fan[19], K. Fang[40], K. Farrag[16], A. R. Fazely[7], A. Fedynitch[57], N. Feigl[10], S. Fiedlschuster[26], C. Finley[54], L. Fischer[63], D. Fox[59], A. Franckowiak[11], A. Fritz[41], P. Fürst[1], J. Gallagher[39], E. Ganster[1], A. Garcia[14], L. Gerhardt[9], A. Ghadimi[58], C. Glaser[61], T. Glauch[27], T. Glüsenkamp[26, 61], N. Goehlke[32], J. G. Gonzalez[44], S. Goswami[58], D. Grant[24], S. J. Gray[19], O. Gries[1], S. Griffin[40], S. Griswold[52], K. M. Groth[22], C. Günther[1], P. Gutjahr[23], C. Haack[26], A. Hallgren[61], R. Halliday[24], L. Halve[1], F. Halzen[40], H. Hamdaoui[55], M. Ha Minh[27], K. Hanson[40], J. Hardin[15], A. A. Harnisch[24], P. Hatch[33], A. Haungs[31], K. Helbing[62], J. Hellrung[11], F. Henningsen[27], L. Heuermann[1], N. Heyer[61], S. Hickford[62], A. Hidvegi[54], C. Hill[16], G. C. Hill[2], K. D. Hoffman[19], S. Hori[40], K. Hoshina[40, 66], W. Hou[31], T. Huber[31], K. Hultqvist[54], M. Hünnefeld[23], R. Hussain[40], K. Hymon[23], S. In[56], A. Ishihara[16], M. Jacquart[40], O. Janik[1], M. Jansson[54], G. S. Japaridze[5], M. Jeong[56], M. Jin[14], B. J. P. Jones[4], D. Kang[31], W. Kang[56], X. Kang[49], A. Kappes[43], D. Kappesser[41], L. Kardum[23], T. Karg[63], M. Karl[27], A. Karle[40], U. Katz[26], M. Kauer[40], J. L. Kelley[40], A. Khatee Zathul[40], A. Kheirandish[34, 35], J. Kiryluk[55], S. R. Klein[8, 9], A. Kochocki[24], R. Koirala[44], H. Kolanoski[10], T. Kontrimas[27], L. Köpke[41], C. Kopper[26], D. J. Koskinen[22], P. Koundal[31], M. Kovacevich[49], M. Kowalski[10, 63], T. Kozynets[22], J. Krishnamoorthi[40, 64], K. Kruiswijk[37], E. Krupczak[24], A. Kumar[63], E. Kun[11], N. Kurahashi[49], N. Lad[63], C. Lagunas Gualda[63], M. Lamoureux[37], M. J. Larson[19], S. Latseva[1], F. Lauber[62], J. P. Lazar[14, 40], J. W. Lee[56], K. Leonard DeHolton[60], A. Leszczyńska[44], M. Lincetto[11], Q. R. Liu[40], M. Liubarska[25], E. Lohfink[41], C. Love[49], C. J. Lozano Mariscal[43], L. Lu[40], F. Lucarelli[28], W. Luszczak[20, 21], Y. Lyu[8, 9], J. Madsen[40], K. B. M. Mahn[24], Y. Makino[40], E. Manao[27], S. Mancina[40, 48], W. Marie Sainte[40], I. C. Mariş[12], S. Marka[46], Z. Marka[46], M. Marsee[58], I. Martinez-Soler[14], R. Maruyama[45], F. Mayhew[24], T. McElroy[25], F. McNally[38], J. V. Mead[22], K. Meagher[40], S. Mechbal[63], A. Medina[21], M. Meier[16], Y. Merckx[13], L. Merten[11], J. Micallef[24], J. Mitchell[7], T. Montaruli[28], R. W. Moore[25], Y. Morii[16], R. Morse[40], M. Moulai[40], T. Mukherjee[31], R. Naab[63], R. Nagai[16], M. Nakos[40], U. Naumann[62], J. Necker[63], A. Negi[4], M. Neumann[43], H. Niederhausen[24], M. U. Nisa[24], A. Noell[1], A. Novikov[44], S. C. Nowicki[24], A. Obertacke Pollmann[16], V. O'Dell[40], M. Oehler[31], B. Oeyen[29], A. Olivas[19], R. Ørsøe[27], J. Osborn[40], E. O'Sullivan[61], H. Pandya[44], N. Park[33], G. K. Parker[4], E. N. Paudel[44], L. Paul[42, 50], C. Pérez de los Heros[61], J. Peterson[40], S. Philippen[1], A. Pizzuto[40], M. Plum[50], A. Pontén[61], Y. Popovych[41], M. Prado Rodriguez[40], B. Pries[24], R. Procter-Murphy[19], G. T. Przybylski[9], C. Raab[37], J. Rack-Helleis[41], K. Rawlins[3], Z. Rechav[40], A. Rehman[44], P. Reichherzer[11], G. Renzi[12], E. Resconi[27], S. Reusch[63], W. Rhode[23], B. Riedel[40], A. Rifaie[1], E. J. Roberts[2], S. Robertson[8, 9], S. Rodan[56], G. Roellinghoff[56], M. Rongen[26], C. Rott[53, 56], T. Ruhe[23], L. Ruohan[27], D. Ryckbosch[29], I. Safa[14, 40], J. Saffer[32], D. Salazar-Gallegos[24], P. Sampathkumar[31], S. E. Sanchez Herrera[24], A. Sandrock[62], M. Santander[58], S. Sarkar[25], S. Sarkar[47], J. Savelberg[1], P. Savina[40], M. Schaufel[1], H. Schieler[31], S. Schindler[26], L. Schlickmann[1], B. Schlüter[43], F. Schlüter[12], N. Schmeisser[62], T. Schmidt[19], J. Schneider[26], F. G. Schröder[31, 44], L. Schumacher[26], G. Schwefer[1], S. Sclafani[19], D. Seckel[44], M. Seikh[36], S. Seunarine[51], R. Shah[49], A. Sharma[61], S. Shefali[32], N. Shimizu[16], M. Silva[40], B. Skrzypek[14], B. Smithers[4], R. Snihur[40], J. Soedingrekso[23], A. Søgaard[22], D. Soldin[32], P. Soldin[1], G. Sommani[11], C. Spannfellner[27], G. M. Spiczak[51], C. Spiering[63], M. Stamatikos[21], T. Stanev[44], T. Stezelberger[9], T. Stürwald[62], T. Stuttard[22], G. W. Sullivan[19], I. Taboada[6], S. Ter-Antonyan[7], M. Thiesmeyer[1], W. G. Thompson[14], J. Thwaites[40], S. Tilav[44], K. Tollefson[24], C. Tönnis[56], S. Toscano[12], D. Tosi[40], A. Trettin[63], C. F. Tung[6], R. Turcotte[31], J. P. Twagirayezu[24], B. Ty[40], M. A. Unland Elorrieta[43], A. K. Upadhyay[40, 64], K. Upshaw[7], N. Valtonen-Mattila[61], J. Vandenbroucke[40], N. van Eijndhoven[13], D. Vannerom[15], J. van Santen[63], J. Vara[43], J. Veitch-Michaelis[40], M. Venugopal[31], M. Vereecken[37], S. Verpoest[44], D. Veske[46], A. Vijai[19], C. Walck[54], C. Weaver[24], P. Weigel[15], A. Weindl[31], J. Weldert[60], C. Wendt[40], J. Werthebach[23], M. Weyrauch[31], N. Whitehorn[24], C. H. Wiebusch[1], N. Willey[24], D. R. Williams[58], L. Witthaus[23], A. Wolf[1], M. Wolf[27], G. Wrede[26], X. W. Xu[7], J. P. Yanez[25], E. Yildizci[40], S. Yoshida[16], R. Young[36], F. Yu[14], S. Yu[24], T. Yuan[40], Z. Zhang[55], P. Zhelnin[14], M. Zimmerman[40]

[1] III. Physikalisches Institut, RWTH Aachen University, D-52056 Aachen, Germany
[2] Department of Physics, University of Adelaide, Adelaide, 5005, Australia
[3] Dept. of Physics and Astronomy, University of Alaska Anchorage, 3211 Providence Dr., Anchorage, AK 99508, USA
[4] Dept. of Physics, University of Texas at Arlington, 502 Yates St., Science Hall Rm 108, Box 19059, Arlington, TX 76019, USA
[5] CTSPS, Clark-Atlanta University, Atlanta, GA 30314, USA
[6] School of Physics and Center for Relativistic Astrophysics, Georgia Institute of Technology, Atlanta, GA 30332, USA
[7] Dept. of Physics, Southern University, Baton Rouge, LA 70813, USA
[8] Dept. of Physics, University of California, Berkeley, CA 94720, USA
[9] Lawrence Berkeley National Laboratory, Berkeley, CA 94720, USA
[10] Institut für Physik, Humboldt-Universität zu Berlin, D-12489 Berlin, Germany
[11] Fakultät für Physik & Astronomie, Ruhr-Universität Bochum, D-44780 Bochum, Germany
[12] Université Libre de Bruxelles, Science Faculty CP230, B-1050 Brussels, Belgium

PoS(ICRC2023)366

[13] Vrije Universiteit Brussel (VUB), Dienst ELEM, B-1050 Brussels, Belgium
[14] Department of Physics and Laboratory for Particle Physics and Cosmology, Harvard University, Cambridge, MA 02138, USA
[15] Dept. of Physics, Massachusetts Institute of Technology, Cambridge, MA 02139, USA
[16] Dept. of Physics and The International Center for Hadron Astrophysics, Chiba University, Chiba 263-8522, Japan
[17] Department of Physics, Loyola University Chicago, Chicago, IL 60660, USA
[18] Dept. of Physics and Astronomy, University of Canterbury, Private Bag 4800, Christchurch, New Zealand
[19] Dept. of Physics, University of Maryland, College Park, MD 20742, USA
[20] Dept. of Astronomy, Ohio State University, Columbus, OH 43210, USA
[21] Dept. of Physics and Center for Cosmology and Astro-Particle Physics, Ohio State University, Columbus, OH 43210, USA
[22] Niels Bohr Institute, University of Copenhagen, DK-2100 Copenhagen, Denmark
[23] Dept. of Physics, TU Dortmund University, D-44221 Dortmund, Germany
[24] Dept. of Physics and Astronomy, Michigan State University, East Lansing, MI 48824, USA
[25] Dept. of Physics, University of Alberta, Edmonton, Alberta, Canada T6G 2E1
[26] Erlangen Centre for Astroparticle Physics, Friedrich-Alexander-Universität Erlangen-Nürnberg, D-91058 Erlangen, Germany
[27] Technical University of Munich, TUM School of Natural Sciences, Department of Physics, D-85748 Garching bei München, Germany
[28] Département de physique nucléaire et corpusculaire, Université de Genève, CH-1211 Genève, Switzerland
[29] Dept. of Physics and Astronomy, University of Gent, B-9000 Gent, Belgium
[30] Dept. of Physics and Astronomy, University of California, Irvine, CA 92697, USA
[31] Karlsruhe Institute of Technology, Institute for Astroparticle Physics, D-76021 Karlsruhe, Germany
[32] Karlsruhe Institute of Technology, Institute of Experimental Particle Physics, D-76021 Karlsruhe, Germany
[33] Dept. of Physics, Engineering Physics, and Astronomy, Queen's University, Kingston, ON K7L 3N6, Canada
[34] Department of Physics & Astronomy, University of Nevada, Las Vegas, NV, 89154, USA
[35] Nevada Center for Astrophysics, University of Nevada, Las Vegas, NV 89154, USA
[36] Dept. of Physics and Astronomy, University of Kansas, Lawrence, KS 66045, USA
[37] Centre for Cosmology, Particle Physics and Phenomenology - CP3, Université catholique de Louvain, Louvain-la-Neuve, Belgium
[38] Department of Physics, Mercer University, Macon, GA 31207-0001, USA
[39] Dept. of Astronomy, University of Wisconsin–Madison, Madison, WI 53706, USA
[40] Dept. of Physics and Wisconsin IceCube Particle Astrophysics Center, University of Wisconsin–Madison, Madison, WI 53706, USA
[41] Institute of Physics, University of Mainz, Staudinger Weg 7, D-55099 Mainz, Germany
[42] Department of Physics, Marquette University, Milwaukee, WI, 53201, USA
[43] Institut für Kernphysik, Westfälische Wilhelms-Universität Münster, D-48149 Münster, Germany
[44] Bartol Research Institute and Dept. of Physics and Astronomy, University of Delaware, Newark, DE 19716, USA
[45] Dept. of Physics, Yale University, New Haven, CT 06520, USA
[46] Columbia Astrophysics and Nevis Laboratories, Columbia University, New York, NY 10027, USA
[47] Dept. of Physics, University of Oxford, Parks Road, Oxford OX1 3PU, United Kingdom
[48] Dipartimento di Fisica e Astronomia Galileo Galilei, Università Degli Studi di Padova, 35122 Padova PD, Italy
[49] Dept. of Physics, Drexel University, 3141 Chestnut Street, Philadelphia, PA 19104, USA
[50] Physics Department, South Dakota School of Mines and Technology, Rapid City, SD 57701, USA
[51] Dept. of Physics, University of Wisconsin, River Falls, WI 54022, USA
[52] Dept. of Physics and Astronomy, University of Rochester, Rochester, NY 14627, USA
[53] Department of Physics and Astronomy, University of Utah, Salt Lake City, UT 84112, USA
[54] Oskar Klein Centre and Dept. of Physics, Stockholm University, SE-10691 Stockholm, Sweden
[55] Dept. of Physics and Astronomy, Stony Brook University, Stony Brook, NY 11794-3800, USA
[56] Dept. of Physics, Sungkyunkwan University, Suwon 16419, Korea
[57] Institute of Physics, Academia Sinica, Taipei, 11529, Taiwan
[58] Dept. of Physics and Astronomy, University of Alabama, Tuscaloosa, AL 35487, USA
[59] Dept. of Astronomy and Astrophysics, Pennsylvania State University, University Park, PA 16802, USA
[60] Dept. of Physics, Pennsylvania State University, University Park, PA 16802, USA
[61] Dept. of Physics and Astronomy, Uppsala University, Box 516, S-75120 Uppsala, Sweden
[62] Dept. of Physics, University of Wuppertal, D-42119 Wuppertal, Germany
[63] Deutsches Elektronen-Synchrotron DESY, Platanenallee 6, 15738 Zeuthen, Germany
[64] Institute of Physics, Sachivalaya Marg, Sainik School Post, Bhubaneswar 751005, India
[65] Department of Space, Earth and Environment, Chalmers University of Technology, 412 96 Gothenburg, Sweden
[66] Earthquake Research Institute, University of Tokyo, Bunkyo, Tokyo 113-0032, Japan

Acknowledgements

The authors gratefully acknowledge the support from the following agencies and institutions: USA – U.S. National Science Foundation-Office of Polar Programs, U.S. National Science Foundation-Physics Division, U.S. National Science Foundation-EPSCoR, Wisconsin Alumni Research Foundation, Center for High Throughput Computing (CHTC) at the University of Wisconsin–Madison, Open Science

PoS(ICRC2023)366

Grid (OSG), Advanced Cyberinfrastructure Coordination Ecosystem: Services & Support (ACCESS), Frontera computing project at the Texas Advanced Computing Center, U.S. Department of Energy-National Energy Research Scientific Computing Center, Particle astrophysics research computing center at the University of Maryland, Institute for Cyber-Enabled Research at Michigan State University, and Astroparticle physics computational facility at Marquette University; Belgium – Funds for Scientific Research (FRS-FNRS and FWO), FWO Odysseus and Big Science programmes, and Belgian Federal Science Policy Office (Belspo); Germany – Bundesministerium für Bildung und Forschung (BMBF), Deutsche Forschungsgemeinschaft (DFG), Helmholtz Alliance for Astroparticle Physics (HAP), Initiative and Networking Fund of the Helmholtz Association, Deutsches Elektronen Synchrotron (DESY), and High Performance Computing cluster of the RWTH Aachen; Sweden – Swedish Research Council, Swedish Polar Research Secretariat, Swedish National Infrastructure for Computing (SNIC), and Knut and Alice Wallenberg Foundation; European Union – EGI Advanced Computing for research; Australia – Australian Research Council; Canada – Natural Sciences and Engineering Research Council of Canada, Calcul Québec, Compute Ontario, Canada Foundation for Innovation, WestGrid, and Compute Canada; Denmark – Villum Fonden, Carlsberg Foundation, and European Commission; New Zealand – Marsden Fund; Japan – Japan Society for Promotion of Science (JSPS) and Institute for Global Prominent Research (IGPR) of Chiba University; Korea – National Research Foundation of Korea (NRF); Switzerland – Swiss National Science Foundation (SNSF); United Kingdom – Department of Physics, University of Oxford.

PoS(ICRC2023)366